Resistance Switching in Large-Area Vertical Junctions of the Molecular Spin Crossover Complex $[Fe(HB(tz)_3)_2]$: ON/OFF Ratios and Device Stability

Yuteng Zhang,[1,2] Isabelle Séguy,[2] Karl Ridier,[1] Victoria Shalabaeva,[1] Mario Piedrahita-Bello,[1] Aurelian Rotaru,[3] Lionel Salmon,[1] Gábor Molnár,[1,*] Azzedine Bousseksou[1,*]

[1] LCC, CNRS and Université de Toulouse, Toulouse, France
[2] LAAS, CNRS and Université de Toulouse, INSA, UPS, F-31077 Toulouse, France
[3] Faculty of Electrical Engineering and Computer Science and MANSiD Research Center, Stefan cel Mare University, Suceava, Romania

E-mail: gabor.molnar@lcc-toulouse.fr and azzedine.bousseksou@lcc-toulouse.fr

Received xxxxxx
Accepted for publication xxxxxx
Published xxxxxx

Abstract

Multilayer crossbar junctions composed of ITO/[Fe(HB(1,2,4-triazol-1-yl)$_3$)$_2$]/M (with M = Al or Ca) were fabricated and investigated for their resistance switching properties. Current–voltage–temperature maps revealed ON/OFF resistance ratios as high as 400, with the ON and OFF states defined, respectively, as the low-resistance, low spin state and the high-resistance, high spin state of the spin crossover layer. Similar results were obtained with Al and Ca cathodes indicating that the charge transport in the insulating spin crossover film is at the origin of the resistance switching instead of electron injection at the electrodes. The reproducibility and stability of the device properties were also studied.

Keywords: spin crossover, multilayer junctions, resistance switching

1. Introduction

Molecular spin crossover (SCO) complexes of certain transition metal ions are well known to exhibit reversible switching between their low spin (LS) and high spin (HS) electronic configurations [1-5]. The transition between the two spin states can be triggered by various external stimuli such as temperature, pressure, light or X-ray irradiation, an intense magnetic field or the inclusion of guest molecules. The SCO is accompanied by a spectacular change of the magnetic, optical, mechanical and electrical properties of the material, which creates opportunities for employing SCO molecules in various technological fields [6, 7].

A number of recent works focus on the potential use of these functional property changes in SCO-based electronic devices. Most of these SCO devices are either horizontal (i.e. current-in-plane) or single molecule junctions [8], but recently vertical (i.e. current out-of-plane) SCO devices have been also successfully fabricated. Actually, the first vertical metal-insulator-metal (MIM) devices containing SCO molecules were reported by Matsuda and co-workers [9-11]. These devices consisted of the stack ITO/$[Fe(dpp)_2](BF_4)_2$:L/Al (ITO = indium tin oxide, dpp = 2,6-di(pyrazol-1-yl)pyridine, L = chlorophyll-a or nile red) and alternatively a hole transport layer (poly(N-vinylcarbazole)) was also deposited between the ITO electrode and the active layer. These devices were investigated for the interplay between their SCO and electroluminescence properties, but to our best knowledge, the charge transport properties have not been reported. More recently, the SCO compound $[Fe(H_2B(pz)_2)_2(phen)]$ **1** (pz = pyrazol-1-yl and phen = 1,10- phenanthroline) was integrated in large-area crossbar devices with the tri-layer structure of ITO/**1**/Al [12]. This work provided a well-reproducible protocol to investigate the switching property of SCO layers of various thickness. The thinnest junctions (ca. 10 nm) showed tunneling behavior between 5 – 300 K, while the thicker SCO layers (ca. 30 – 200 nm) gave rise to a diode-like rectifying behavior and thermal activation of the conductance. In both type of devices, the thickness dependence of the electrical properties indicated that the transport is primarily limited by the low conductance of the SCO films. Typically, the switching from the LS to the HS state led to a drop of the resistance by ca. 10 - 50 % (i.e. ON/OFF < 2). The same device structure was also achieved with thin films of the SCO complex $[Fe(HB(tz)_3)_2]$ (tz = 1,2,4-triazol-1-yl) **2**. The charge transport mechanism in junctions with different thicknesses (10, 30, 100 and 200 nm) was studied and an ON/OFF current ratio of ca. 8 was found when switching the molecules from the LS to the HS state [13]. The same compounds, **1** [14] and **2** [15], were also used to construct multilayer junctions with the structure of Au/SCO/EGaIn, which exhibited ON/OFF current ratios of ca. 10 and 100, respectively, upon the SCO. Interestingly, the HS state appeared more conducting in these devices, which the authors rationalized in the frame of the Simmons' tunneling model by taking into account the variation of frontier molecular orbital energies upon the SCO. In any case, this finding indicates that the influence of SCO on the device resistance can strongly differ depending on the charge transport mechanism. The same group also succeeded in constructing crossbar devices using the evaporable SCO complex $[Fe(qnal)_2]$ (qnal = quinoline-naphthaldehyde) **3** between silver and gold electrodes [16] and a correlation between the LS to HS conversion and the decrease of the device resistance was pointed out. Thin films (ca. 40 nm) of the amino derivative of **1**, the complex $[Fe(H_2B(pz)_2)_2(NH_2\text{-}phen)]$ **4**, were also investigated in a Au/**4**/Au crossbar configuration [17]. Interestingly, a relatively small change of the HS/LS fractions could be correlated with a significant change of the device resistance. In addition, the role of sample heterogeneity in the charge transport was highlighted using an operando x-ray absorption spectroscopy method.

These different results with out-of-plane devices together with the most relevant planar junctions are summarized in Table 1. One can remark that the ON/OFF current ratios appear in general rather low, but it is fair to say that the number of investigated SCO compounds and devices remains also rather restricted. Yet, in a few cases, more promising 2-3 orders of magnitude changes of the device resistance could be detected. It is interesting to observe also that the same SCO compound may give rise to very different characteristics, depending on the device structure. A tangible correlation between the SCO and the current switching phenomena remains, however, problematic in several cases as it relies on the ex-situ evaluation of the spin-crossover properties. Finally, we shall note that, in general, there is only few (or no) mention about 'statistics' in the publications, i.e. the reproducibility of the fabrication process, the reversibility of the current switching (cycle numbers) and the lifetime of the devices. This aspect certainly deserves to be bolstered in future reports.

In this paper, we report on a more comprehensive investigation of our previously reported [13] multilayer junctions of the SCO compound **2**. Along the above lines, we performed a more detailed study of current-voltage-temperature characteristics of these junctions. We explored also the possibility of electrode work function tuning and developed effective solutions to reduce problems associated with device degradation and aging. These efforts allowed us to optimize the experimental conditions leading to a resistance switching with ON/OFF ratios up to 400.

2. Experimental details

The device fabrication followed our previous work [13]. Before the fabrication, the ITO substrates (CEC010S from Praezisions Glas & Optic GmbH) were rinsed successively by acetone (VLSI, 99.5%) and ethanol (VLSI, 99.9%) for 5 minutes under sonication. The substrates were dried by an argon gas flow. Then, a 100 nm thick film of **2** was deposited by thermal evaporation at 180 °C under high vacuum (2.7×10^{-7} mbar) at a rate of ca. 0.3 Å/s, followed by water-vapor annealing in ca. 80 % relative humidity air at room temperature for 10 min. As it was shown previously [13], this post-deposition treatment allows for high quality, oriented, nanocrystalline films of **2**. Finally, a 100 nm thick Al film was deposited through a shadow mask under a vacuum pressure of about 3.0×10^{-6} mbar at a rate of 10 Å/s to form the upper electrodes of the ITO/**2**/Al stack. A rotating substrate holder was used for both organic and metallic deposition to improve film thickness uniformity. In addition, to avoid any organic layer damage during the top electrode fabrication, the sample temperature was maintained below 30 °C by a water-cooled substrate holder. The effective junction area is ca. 3 mm^2. Alternatively, the top electrode was made of Ca, which was deposited at a vacuum pressure of 2.6×10^{-7} mbar at a rate of 2.7 Å/s. Contrary to the Al devices, the Ca devices were encapsulated by an epoxy resist (*vide infra*) to protect them from oxydation and, finally, silver paste was attached to the ITO electrodes to establish good electrical connection. Current-voltage and current-temperature characteristics of the junctions were analyzed using a Keithley-6430 source-meter and a heating-cooling probe station (Linkam Scientific HFS350EV-PB4) equipped with gold-tipped tungsten probes.

Table 1. Current switching properties reported for various SCO junctions

Ref.	SCO compound	Device structure	Current LS (A)	Current HS (A)	ON/OFF ratio
12	$[Fe(H_2B(pz)_2)_2(phen)]$ film	ITO/SCO/Al	2.0×10^{-9}	1.0×10^{-9}	2
13	$[Fe(HB(tz)_3)_2]$ film	ITO/SCO/Al	5.0×10^{-6}	6.0×10^{-7}	8
14	$[Fe(H_2B(pz)_2)_2(phen)]$ film	Au/SCO/EGaIn	3×10^{-10}	3×10^{-9}	10*
15	$[Fe(HB(tz)_3)_2]$ film	Au/SCO/EGaIn	3×10^{-8}	3×10^{-6}	100
17	$[Fe(H_2B(pz)_2)_2(NH_2\text{-phen})]$ film	Au/ SCO/Au	8×10^{-8}	8×10^{-6}	100*
18	$[Fe(Htrz)_2(trz)](BF_4)$ nanorods	Au/ SCO/Au	2.6×10^{-8}	1.5×10^{-8}	1.7
19	$[Fe(Htrz)_2(trz)](BF_4)$ nanoparticles	Au/ SCO/Au	1×10^{-9}	3×10^{-12}	300
20	Au@$[Fe(Htrz)_2(trz)](BF_4)$ particles	Au/ SCO/Au	6×10^{-9}	4×10^{-12}	1500
21	$[Fe(trz)_3](BF_4)_2$ nanoparticles	Au/ SCO/Au	2.6×10^{-10}	8.8×10^{-10}	2.4
22	$[Fe(trz)_3](BF_4)_2$ nanoparticles	Graphene-based	1×10^{-6}	2×10^{-6}	2
23	$[Fe(trz)_3](BF_4)_2$ nanoparticles	Graphene-based	3×10^{-10}	3×10^{-11}	10
This work	$[Fe(HB(tz)_3)_2]$ thin film	ITO/SCO/Al	4.2×10^{-8}	1×10^{-10}	400
This work	$[Fe(HB(tz)_3)_2]$ thin film	ITO/SCO/Ca	2.0×10^{-5}	3.9×10^{-7}	50

* In these junctions, it is difficult to separate the contributions to the ON/OFF ratio arising from the rather gradual SCO and from the ordinary thermal activation of the conductivity.

Table 2. Comparison of the room temperature electrical resistance of a batch of ITO/100 nm $[Fe(HB(tz)_3)_2]$/Al junctions

Device n°	1	2	3	4	5	6	7	8	9	10	11	12
Resistance (MΩ)	3.7	2.7	2.5	3.4	3.0	2.7	3.5	2.8	2.5	3.0	3.1	2.8
Device n°	13	14	15	16	17	18	19	20	21	22	23	24
Resistance (MΩ)	3.4	2.9	2.7	3.4	3.1	2.8	3.2	2.7	2.3	3.3	3.0	2.6

3. Results and discussion

The morphology as well as thickness of the SCO films were analyzed by atomic force microscopy (AFM) in tapping mode. As shown in Figure 1, the measured film thickness (99 ± 4 nm) matches well the nominal thickness (100 nm). The film appears dense, homogeneous and smooth with a root-mean-squared roughness of ca. 1 nm.

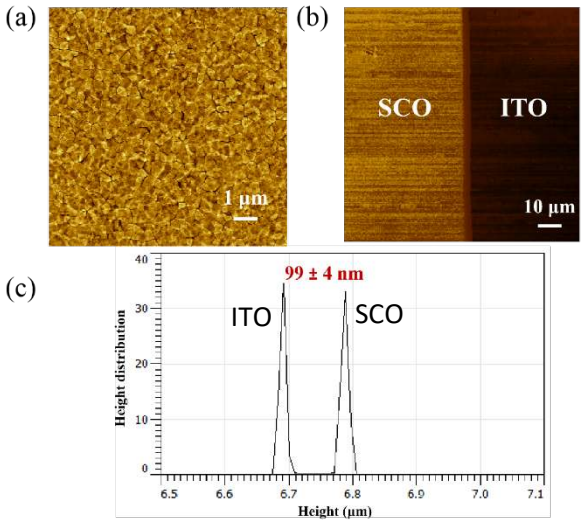

Figure 1. a) 10×10 µm AFM topography image of a [Fe(HB(tz)$_3$)$_2$] thin film. b) 100×100 µm AFM topography image of a [Fe(HB(tz)$_3$)$_2$] thin film and the bare ITO substrate and c) the corresponding height distribution histogram.

The ITO/**2**/Al junctions were first characterized for their room temperature resistance. Table 2 reports the resistance data obtained as the average of three measurements under 1 µA current bias for 24 junctions (on 4 chips). None of the junctions were short-circuited and the mean resistance value of 3.0 ± 0.4 MΩ is well reproduced device-to-device. The room temperature I-V characteristics averaged for 12 as-prepared devices are shown in Figure 2 (see Figure S1 in the Supplementary Materials for the corresponding individual I-V curves).

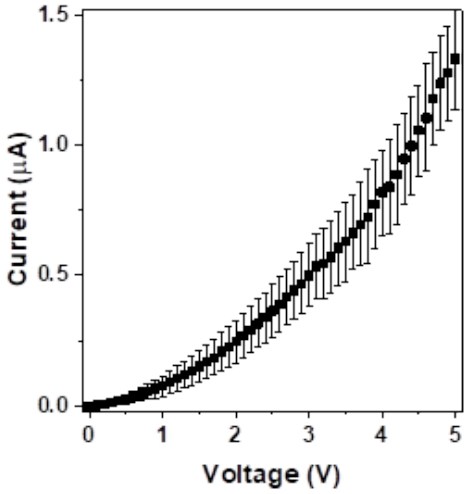

Figure 2. Averaged I-V characteristics of twelve as-prepared ITO/100 nm [Fe(HB(tz)$_3$)$_2$]/Al junctions recorded in ambient conditions at rates of ± 100 mV/s.

Similar to our previous report [13], we found that the I-V curves of the junctions are strongly nonlinear and behave in a reproducible manner only under forward bias, i.e., when the Al electrode is the cathode. The origin of the instability of the junctions under reverse bias remains unclear. On the other hand, the nonlinear shape of the I-V curves arises most likely from a voltage activation of the charge transport. The device-to-device reproducibility of the current value for 5 V applied bias was found ca. 15 %. Similar to the ITO/**1**/Al junctions reported in ref. 12, we observed a temporal evolution of the junction properties on time scales of day/week (see Figure S2), manifested by the slow degradation of the I-V characteristics upon storage – presumably due to the oxydative degradation of Al and/or the modification of the SCO/electrode interfaces.

Figure 3 depicts the temperature dependent I-V and I-T characteristics (insert) of a ITO/**2**/Al junction. (See Fig. S3 for the thermal cycling of another junction.) Figure 3(a), (b), (c) and (d) refers to the first, second, third and fourth successive thermal cycle, respectively, acquired for the same junction. The I- T curves show a weak thermal activation and, in perfect agreement with our previous report [13], a substantial change from a high conductance state to a low conductance state occurs at around 65 °C. Since this resistance switching phenomenon is opposed to the thermal activation of the conductance, we can unambiguously distinguish the two processes and extract properly the ON/OFF switching ratio arising solely from the SCO.

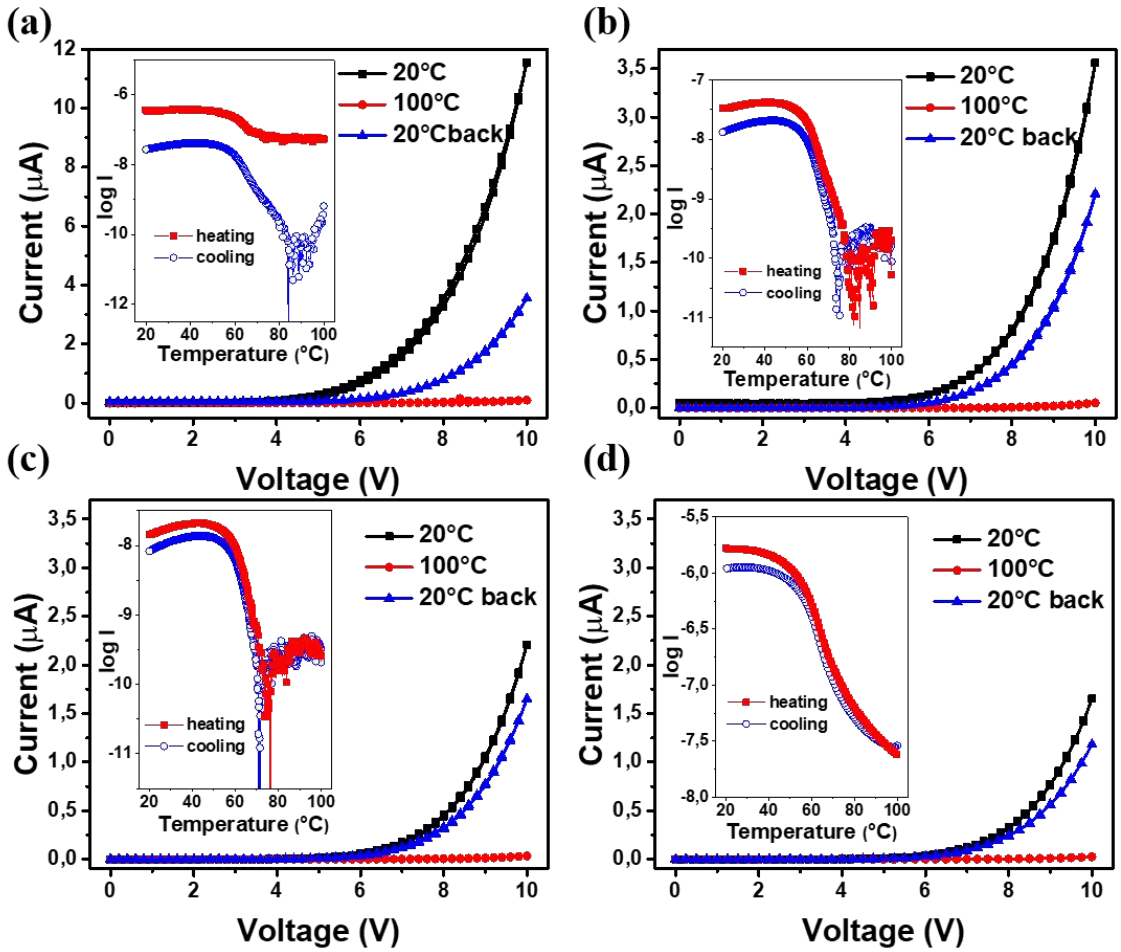

Figure 3. Electrical characteristics of an ITO/100 nm $[Fe(HB(tz)_3)_2]$/Al junction. The results of four successive thermal cycles of an 'as-received' device are showed in (a), (b), (c) and (d). *I-V* curves were recorded at 20 °C and 100 °C and then again at 20 °C at rates of ± 100 mV/s. The inserts show the log *I- T* curves recorded with an applied bias of 5 V for (a-c) and 10 V for (d), at scan rates of ±10 °C/min.

In Figure 3a-d, one can note also that upon successive thermal cycles the junction properties are modified. In particular, the first heating leads always to an anomalous response, but starting from the first cooling curve the device resistance becomes sensibly less affected by the heating-cooling cycle. (N.B. In order to reduce the noise at high temperatures, in the 4th thermal cycle we applied higher voltage, leading obviously to higher current intensities.) This "run-in" effect may be linked to stress relaxation phenomena in the devices. It is important to note that reasonably reproducible device characteristics upon heating could be achieved only by optimizing the experimental conditions. In particular, the measurement reproducibility is increased by applying only low bias (5 V) and by reducing the exposure of the junctions to high temperatures. This latter condition was achieved by limiting the temperature span to 100 °C and increasing the scan rate to 10 K/min. However, it is fair to say that despite all our efforts each investigated junction showed continuous ageing, which was accelerated by thermal/voltage cycling.

The data in Figure 3 reveal another important finding. In contrast to the previously reported ON/OFF ratio of 8 (i.e. ca. one order of magnitude switching), in the present experiments the resistance changes reach 2-3 orders of magnitude in several devices, with ON/OFF ratios up to 400. We believe that this spectacular improvement of ON/OFF switching ratios, with respect to the devices reported in reference 13, is likely related to the more careful handling of the devices in terms of exposure to air, high voltages and high temperatures. Another important issue here is the strong nonlinearity of the I-V curves. As shown in Figure 4 (see also Figure S4), when switching from the LS to the HS state, the current intensity drops by the same factor (ON/OFF ≈ 100) in the high voltage regime (> ca. 6.5 V), wherein both the HS and LS conductions are effectively voltage activated. On the other hand, at low bias (< ca. 4 V) the conduction vanishes in both spin states. There exists however, an intermediate voltage range between ca. 4 - 6.5 V wherein the LS conduction is activated, whereas the HS state remains strongly resistive. In this voltage window, we observe a peak ON/OFF = 400 switching ratio, which arises clearly from the decrease of the turn-on voltage when going from the HS to the LS state. (N.B. The peak ON/OFF ratio we observe here is limited by the dark current as well as by the noise floor of our electrometer.)

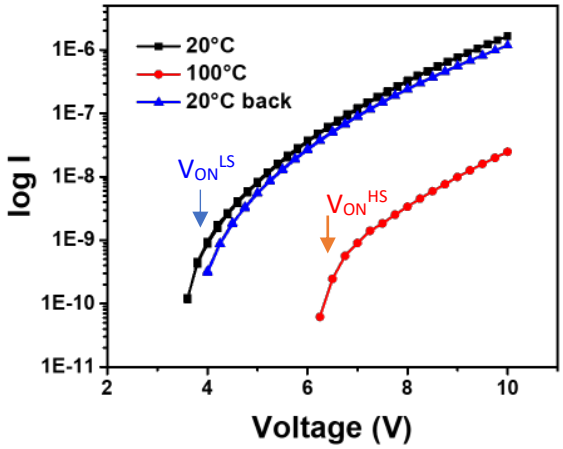

Figure 4. Log *I*-*V* representation of a ITO/100 nm [Fe(HB(tz)$_3$)$_2$]/Al device characteristics at different temperatures evidencing a shift of the turn-on voltage (V_{on}) between the LS (20°C) and HS (100 °C) states. (Same data as in Fig. 3d.)

From the thickness dependence of the current intensity vs. applied field characteristics, we have previously suggested that the charge transport in the ITO/**2**/Al junctions, with thickness in the 100-200 nm range, is limited by the bulk conduction of the SCO layer [13]. To further examine this issue, we decided to investigate the influence of the cathode material on the device properties. Aluminum and calcium are frequently used as electrodes in organic electronics. These two metals are characterized by very different work functions (WF_{Al} = 4.3 eV, WF_{Ca} = 2.9 eV) and allow thus for largely different device characteristics in terms of electron injection properties. Al is reasonably stable in air, but Ca would be quickly oxidized in ambient environment and isolating the device from the external environment by encapsulation becomes mandatory. Based on the established junction structure, we have put in place a simple encapsulation protocol (Figure 5). After the Ca electrodes were deposited, the junctions were transferred from the evaporator to a glove box (O_2/H_2O < 5 ppm) and a thin layer of epoxy resist was coated carefully around the junctions, taking care to not contaminate the SCO layer. A clean glass slide was placed on top of the epoxy layer, which was then cured under UV irradiation for 20 min. The quality of the encapsulation was confirmed by following the I-V characteristics in ambient air for a week (see Fig. S2b).

Figure 6 depicts temperature-dependent I-V and I-T characteristics of an encapsulated ITO/**2**/Ca junction. These measurements were conducted in ambient atmosphere without additional protection. Figures 6(a) and 6(b) refer to the first and second successive thermal cycles, respectively (see also Figure S5). The ON/OFF current ratio reaches a value of 50, which is comparable in magnitude with the devices made with Al cathode. The I-V curves are also similar for the two types of devices,

but the current intensity is higher in the Ca-based devices. We can thus conclude that decreasing the electron injection energy barrier between the cathode (from Al to Ca) and the SCO material, as expected, electron injection is facilitated, but this does not affect considerably the resistance switching properties. This finding seems to corroborate our hypothesis that the resistance switching phenomenon is related to the hopping-type charge transport in the SCO film. Different explanations, such as Fermi-level pinning at the molecule-electrode interface [24] and/or the pinning of the spin states of molecules adsorbed on the electrodes [7] may account for the lack of influence of the electrode-molecule interface on the resistance switching properties. Surprisingly, the spin transition in the Ca-based devices is associated with a much wider hysteresis loop than for the Al-based devices or for the neat SCO films of compound **2** [13]. We speculate that this phenomenon may be linked to the less effective dehydration of the SCO film in the encapsulated device following the water vapor annealing step.

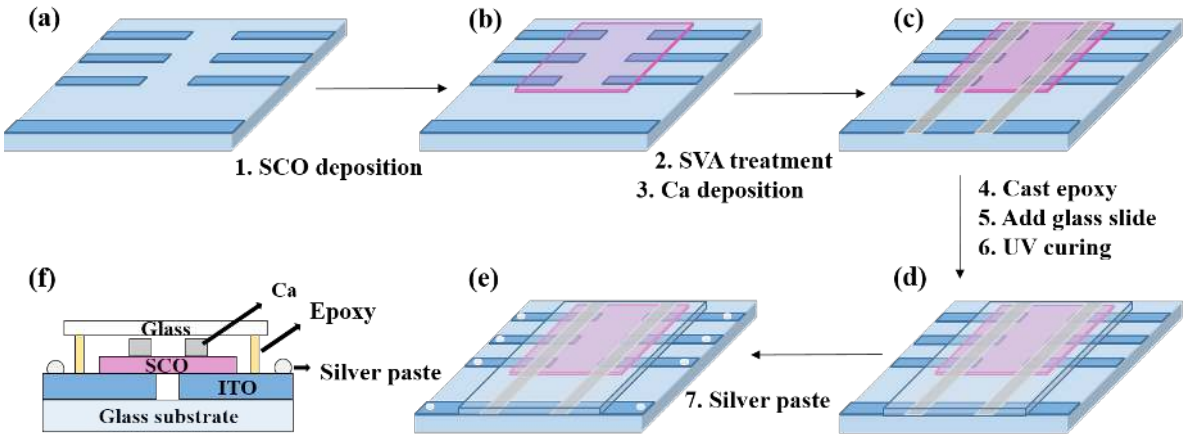

Figure 5. Scheme of the fabrication of encapsulated ITO/100 nm $[Fe(HB(tz)_3)_2]$/Ca junctions.

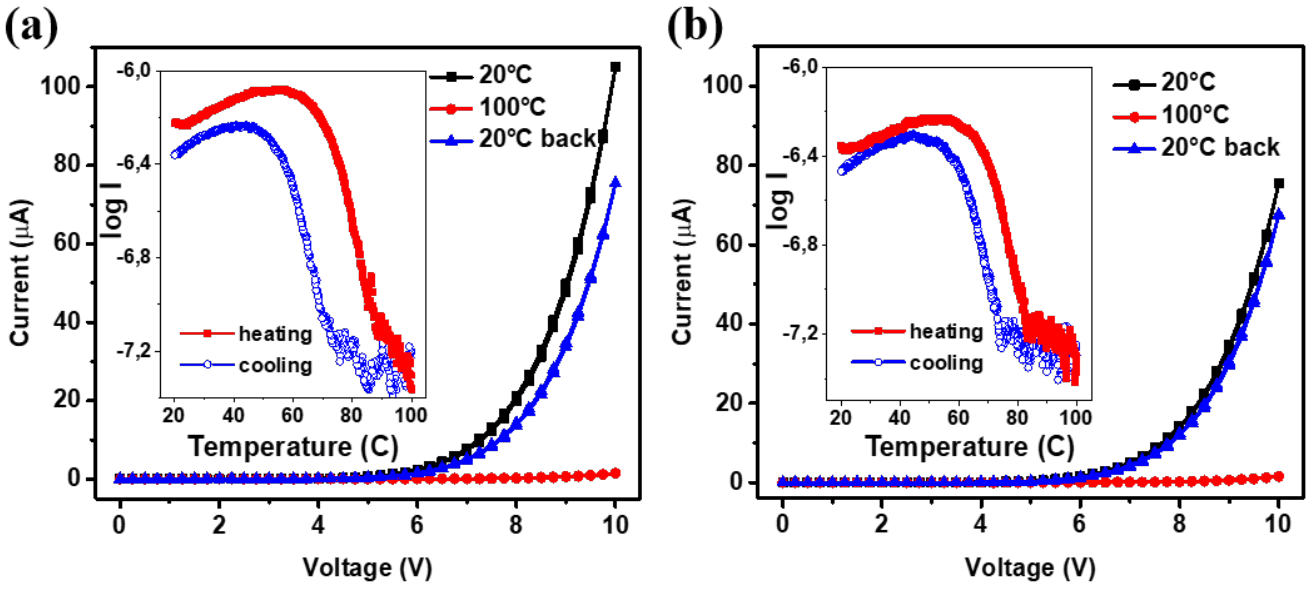

Figure 6. Electrical characteristics of an ITO/100 nm $[Fe(HB(tz)_3)_2]$/Ca junction. The results of two successive thermal cycles of the 'as-received' devices are showed in (a) and (b). *I-V* curves were recorded at 20 °C and 100 °C and then again at 20 °C at rates of ± 100 mV/s. The inserts show the log *I- T* curves recorded with an applied bias of 5 V at scan rates of ±10 °C/min (a) and ±5 °C/min (b).

4. Conclusions

In summary, we have fabricated in a well-reproducible manner, large-area crossbar junctions with ITO/SCO/Metal multilayer structure, integrating high-quality [Fe(HB(1,2,4-triazol-1-yl)$_3$)$_2$] spin crossover films. The careful handling of of the devices in terms of exposure to high temperature, voltage bias and air allowed us to reach ON/OFF switching ratios of ca. 2 orders of magnitude. Then, taking advantage of the non-linear current-voltage characteristics, we show that there exists a voltage range, delimited by the turn-on voltages in the low spin and high spin states, which allows for maximising the resistance switching (ON/OFF = 400). Despite different metals (Al/Ca) were employed as cathode material, the device characteristics remained similar indicating that electron injection is not the key factor in the resistance switching properties. This latter is most likely linked to the charge transport in the spin crossover film. Device stability upon temperature and voltage cycling remains to be improved – encapsulation appears as a promising appraoch to this aim.

Acknowledgements

This work was financed by the European Commission through the SPINSWITCH project (H2020-MSCA-RISE-2016, Grant Agreement No. 734322). The PhD grants of YZ and MPB were financed by the China Scholarship Council and the Federal University of Toulouse/Occitanie Region. This work was supported by the Micro and Nanotechnologies Platform of LAAS-CNRS (Toulouse, France), which is a member of the French RENATECH Network.

References

[1] Gütlich P, Hauser A and Spiering H 1994 *Angewandte Chemie International Edition in English* **33** 2024.
[2] Spin Crossover in Transition Metal Compounds I–III (Eds. Gütlich P and Goodwin HA), in Topics in Current Chemistry, Springer, Berlin, Germany, 2004.
[3] Spin-Crossover Materials: Properties and Applications (Ed. Halcrow MA), Wiley, Oxford, UK, 2013.
[4] Bousseksou A, Molnár G, Salmon L and Nicolazzi W 2011 *Chemical Society Reviews* **40** 3313.
[5] Spin Crossover Phenomenon (Ed. Bousseksou A), in Compte Rendus Chimie, Elsevier, Amsterdam, The Netherlands, 2018.
[6] Kumar KS and Ruben M 2017 *Coordination Chemistry Reviews* **346** 176.
[7] Molnár G, Rat S, Salmon L, Nicolazzi W and Bousseksou A 2018 *Advanced Materials* **30** 17003862.
[8] Lefter C, Davesne V, Salmon L, Molnár G, Demont P, Rotaru A and Bousseksou A 2016 *Magnetochemistry* **2** 1.
[9] Matsuda M, Isozaki H and Tajima H 2018 *Chemistry Letters* **37** 374.
[10] Matsuda M, Isozaki H and Tajima H 2008 *Thin Solid Films* **517** 1465
[11] Matsuda M, Kiyoshima K, Uchida R, Kinoshita N and Tajima H 2013 *Thin Solid Films* **531** 451.
[12] Lefter C, Rat S, Costa JS, Manrique-Juárez MD, Quintero CM, Salmon L, Séguy I, Leichle T, Nicu L, Demont P and Rotaru A 2016 *Advanced Materials* **28** 7508.
[13] Shalabaeva V, Ridier K, Rat S, Manrique-Juarez MD, Salmon L, Séguy I, Rotaru A, Molnár G and Bousseksou A 2018 *Applied Physics Letters* **112** 013301.
[14] Poggini L, Gonidec M, Balasubramanyam RK, Squillantini L, Pecastaings G, Caneschi A and Rosa P 2019 *Journal of Materials Chemistry C* **7** 5343.
[15] Poggini L, Gonidec M, González-Estefan JH, Pecastaings G, Gobaut B and Rosa P 2018 *Advanced Electronic Materials* **4** 1800204.
[16] L. Poggini et al. Functional device with Spin-Crossover compounds. Conference presentation at the 7th European Conference on Molecular Magnetism, Florence (Italy) 15-19 Sept. 2019.
[17] Schleicher F, Studniarek M, Kumar KS, Urbain E, Katcko K, Chen J, Frauhammer T, Hervé M, Halisdemir U, Kandpal LM, Lacour D, Riminucci A, Joly L, Scheurer F, Gobaut B, Choueikani F, Otero E, Ohresser P, Arabski J, Schmerber G, Wulfhekel W, Beaurepaire E, Weber W, BouKari S, Ruben M and Bowen M 2018 *ACS Applied Materials & Interfaces* **10** 31580.
[18] Rotaru A, Dugay J, Tan RP, Guralskiy IA, Salmon L, Demont P, Carrey J, Molnár G, Respaud M and Bousseksou A. 2013 *Advanced Materials* **25** 1745.
[19] Dugay J, Giménez-Marqués M, Kozlova T, Zandbergen HW, Coronado E and van der Zant HS 2015 *Advanced Materials* **27** 1288.
[20] Torres-Cavanillas R, Sanchis-Gual R, Dugay J, Coronado-Puchau M, Giménez-Marqués M and Coronado E 2019 *Advanced Materials* **18** 1900039.
[21] Prins F, Monrabal-Capilla M, Osorio EA, Coronado E and van der Zant HS 2011 *Advanced Materials* **23** 1545.
[22] Dugay J, Aarts M, Giménez-Marqués M, Kozlova T, Zandbergen HW, Coronado E and Van der Zant HS 2016 *Nano letters* **17** 186.
[23] Holovchenko A, Dugay J, Giménez-Marqués M, Torres-Cavanillas R, Coronado E and van der Zant HS 2016 *Advanced Materials* **28** 7228.

[24] Bokdam M, Çakır D and Brocks G 2011 *Applied Physics Letters* **98** 59.